Monte Carlo Simulations of Nanogels Formation by Intramolecular Recombination of Radicals on Polymer Chain. Dispersive Kinetics Controlled by Chain Dynamics†

Jeremiasz K. Jeszka,‡,§ Slawomir Kadlubowski,⊥ and Piotr Ulanski*,⊥

Centre of Molecular and Macromolecular Studies, Polish Academy of Sciences, Sienkiewicza 112, 90-363 Lodz, Poland; Department of Molecular Physics, Technical University of Lodz, Żwirki 36, 90-924 Lodz, Poland; and Institute of Applied Radiation Chemistry, Technical University of Lodz, Wróblewskiego 15, 93-590 Lodz, Poland

Received August 26, 2005; Revised Manuscript Received November 2, 2005

ABSTRACT: Kinetics of nanogel formation by intramolecular recombination of radicals generated on a linear chain is studied by Monte Carlo simulation using cooperative motion algorithm (CMA) and pulse radiolysis of poly(ethylene oxide) in oxygen-free aqueous solutions. Simulations, in good agreement with experiments, show dispersive kinetics of the process. Simulations of simple model cases (fixed distance between radicals, formation of loops, radical transfer), which are difficult or impossible to investigate experimentally, broaden the understanding of the importance of elementary processes which contribute to kinetics of recombination of randomly distributed radicals on long chains. It is shown that the main factor determining the radical recombination is the distance between them along the chain which strongly favors nearest-neighbor reaction. Decay half-time is related to the average distance between the radicals, but the time dependence of the rate constant (dispersive kinetics) is governed by the number of radicals per chain and chain length and cannot be described by a simple formula in a broad time range. Formation of intramolecular covalent bonds in the recombination process (generation of loops) has no detectable influence on the radical decay kinetics, probably due to the simultaneous occurrence of two opposite phenomena: buildup of steric hindrance and reduction of distance between the radicals. The relationship between decay kinetics and chain relaxation processes is discussed.

Introduction

Cross-linked polymeric materials are nowadays omnipresent in technology and everyday life. One of the methods applied to synthesize such products is the radiation technique. Under the action of ionizing radiation, free radicals are formed on the polymer chains, and their subsequent recombination leads to the formation of covalent bonds between the macromolecules, joining them into a three-dimensional network. This method usually allows to cross-link pure polymers, without a need to introduce any monomers, cross-linking agents, initiators, sensitizers, etc. Besides many large-scale applications where radiation technique is used to cross-link solid polymers (cable insulation, thermoshrinkable materials, rubber, etc.), there is a number of processes where it is applied for cross-linking of hydrophilic polymers in aqueous solutions. In most cases the products are macroscopic, permanent hydrogels, having numerous applications, including soil conditioners, soft contact lenses, matrices for controlled drug delivery, and wound dressings.[1] Studies on mechanistic and kinetic aspects of the underlying chemical processes, i.e., mainly intermolecular cross-linking of polymer-derived radicals in water, have been published for a number of synthetic hydrophilic polymers (for a brief recent review, see ref 2).

Free-radical polymer cross-linking in solution can be also used to synthesize gel particles of micrometer and submicrometer size: microgels and nanogels.[3−6] Actual and potential applications of these products range from fillers in paint formulations to sophisticated biomaterials.[7−11] Efficient application of the radiation method (or any other free-radical-generating procedure) to the synthesis of micro- and nanogels requires the underlying physics and chemistry to be understood in some detail.

Nanogels may be defined as internally cross-linked single macromolecules of molecular weight and dimensions similar to the parent, linear polymer chains, but having a number of transverse covalent bonds between the chain segments. Formation of these bonds requires intramolecular recombination of many radical pairs formed at the same polymer chain. This can be achieved by pulse-irradiating the polymer in a dilute, usually aqueous solution.[3,5,6,12−16] In this way, for high-molecular-weight polymers, it is possible to generate tens or even over a hundred radicals per chain within a microsecond. Since other chains are far away and intercoil encounter requires considerable diffusion time, most of these radicals decay with their neighbors located along the same macromolecule.

Albeit radiation-induced intramolecular cross-linking in polymer solution has been already evidenced nearly 50 years ago,[17] first direct kinetic observations of inter- and intramolecular recombination of radiation-generated polymer-based radicals processes were published much later, after the advent of pulse radiolysis technique. This method (cf. refs 18−21) allows generating radicals in the system by fast electron pulses lasting from nano- to microseconds and following the decay in absorbance of these radicals in nano-, micro-, and millisecond time scales. At first, the attention of researchers was focused on studying the kinetics of intermolecular radical recombination, in the conditions where less than one radical per chain was generated during the pulse. For a number of simple, water-soluble polymers it has been demonstrated that the decay of

† This paper is dedicated to the memory of professor Tadeusz Pakula (1945−2005), whose fundamental contributions to the simulations of polymer chain dynamics made this work possible.

‡ Polish Academy of Sciences.

§ Department of Molecular Physics, Technical University of Lodz.

⊥ Institute of Applied Radiation Chemistry, Technical University of Lodz.

* Corresponding author: e-mail ulanskip@mitr.p.lodz.pl; Ph (++48) 42 631 3184; Fax (++48) 42 684 0043.

10.1021/ma0518757 CCC: $33.50
Published on Web 12/24/2005

the radicals followed classical second-order kinetics.[22,23] The dependence of the recombination rate constants on the chain length may be interpreted in terms of diffusion of coils (according to the Smoluchowski theory) or segmental diffusion. However, when the average number of radicals generated simultaneously on each chain exceeds one and polymer concentration is low (below the critical hydrodynamic concentration), intramolecular recombination dominates and the radical decay significantly deviates from the homogeneous second-order kinetics.

In a study coauthored by one of us, kinetics of radical recombination in oxygen-free aqueous solutions of poly(ethylene oxide) (PEO) has been investigated by pulse radiolysis with spectrophotometric detection.[12]

The main conclusions resulting from the experimental study on the intramolecular decay of PEO radicals[12] were the following:

- The apparent momentary second-order rate constant of the reaction, called in the further text the rate coefficient, decreases in the course of the reaction and therefore the decay cannot be described with classical, homogeneous second-order kinetics.
- The decay rate depends on the initial average number of radicals generated on each chain (Z_0), rather than on the overall radical concentration in the system.
- At high Z_0, the initial rate coefficient can reach values of $2k = 7 \times 10^9$ dm^3 mol^{-1} s^{-1}, i.e., much higher than the rate constants of intermolecular recombination of similar radicals (even for much more mobile PEO oligomers, the latter does not exceed $2k = 5 \times 10^8$ dm^3 mol^{-1} s^{-1} [12,22]).
- The time dependence of the rate coefficient can be satisfactorily approximated by the dispersive kinetics model in the form

$$k = Bt^{\alpha-1} \tag{1}$$

This general equation has been demonstrated to be applicable in a large variety of chemical systems, including polymeric ones (for reviews, see refs 24 and 25). The values of the α parameter in the PEO system, calculated using the second-order kinetics, while being close to 1 for $Z_0 < 1$ (dominating intermolecular recombination, classical kinetics), drop to the range 0.4−0.7 for $Z_0 > 1$ (prevailing intramolecular recombination).

These kinetic effects have been demonstrated for a number of simple water-soluble polymers,[13,15,16,26−29] and therefore they seem to be a general feature of multiple-pair intramolecular recombination of polymer radicals, independent, at least qualitatively, on the chemical structure of the monomer unit.

The above-discussed kinetic model (eq 1) is equivalent to the stretched exponential (eq 2) when first-order k is used ($\beta = \alpha$):

$$\frac{Z(t)}{Z_0} = \exp\left[-\left(\frac{t}{\tau}\right)^{\beta}\right] \tag{2}$$

where $Z(t)$ denotes the average number of radicals per chain at a given reaction time t.

Substituting a second-order rate coefficient into eq 1 yields the following kinetic formula (eq 3):

$$\frac{1}{Z(t)} - \frac{1}{Z_0} = \frac{Bt^{\alpha}}{\alpha} \tag{3}$$

The use of first-order kinetics seems to be justified in systems in which the presence (and eventually recombination) of other radicals does not influence significantly the recombination rate of a close-neighbor pairs which recombine much faster. In particular, in diluted solutions, this is the case when only one radical pair is generated on a chain, and thus the probability of the recombination event does not depend on any previous events in the system (see detailed discussion below).

Several possible explanations of the nonclassical kinetics and of the fact that the momentary rate coefficient decreases in the course of the reaction can be considered. It may be an inherent property of the long time scale (and long distance) chain dynamics. It may also result from the fact that, during the recombination, internal C−C bonds are formed between previously independent chain segments, the structure becomes internally cross-linked and therefore more rigid, and lower segmental mobility slows down further recombination steps. It may be caused by the random distribution of the distances between the generated radicals. It has been also postulated that the distribution of radiation-generated radicals along a chain might be in fact not fully random.[26] Two or three OH radicals formed in one spur may attack polymer chain at neighboring sites, generating groups of polymer radicals in which the radical−radical distances are much smaller than the average.

Experimental studies, however, do not always yield a clear-cut picture allowing for unambiguous explanation of the observed kinetic features (see discussion below). Having billions of chains in the studied real polymer sample, we always deal with various distributions: distribution of chain length, of number of radicals per chain, of mutual interchain distances, etc. There is no way to fully exclude intermolecular processes. Moreover, the possibility to change some of the parameters is limited, either by chemistry and statistics or by technical reasons. One cannot influence the recombination-to-disproportionation ratio, and one cannot generate the radicals along the chain in specific distances or arrangements. On the other hand, it is also not obvious whether we can assume a purely statistical radical generation along the chain.

In this work, we use a Monte Carlo simulation of intramolecular recombination (and disproportionation) of radicals on single polymer chains to broaden our understanding of the kinetics of these processes and to study these aspects that are difficult or impossible to investigate experimentally.

The aim is to get an insight into the origin of the observed nonclassical kinetic behavior (the dispersive kinetics). In particular, we wanted to find out which parameters have a decisive influence on the kinetics of intramolecular radical recombination on molecular level and what is the main reason for the nonclassical kinetic behavior.

For comparison, we preformed experimental studies in which high concentrations of radicals were generated instantaneously at poly(ethylene oxide) chains in oxygen-free aqueous solutions, and their recombination was subsequently followed by time-resolved spectroscopy. Our intention was to verify, on the basis of cases where comparison between simulation and experiment was possible, to what extent the model and algorithm applied in simulations provide a true picture of the real situation (while bearing in mind the technical limitations and assumptions made in the processing of experimental data).

In the second paper we shall present the relationship between the parameters of intramolecular radical recombination and the structure of the final products—nanogels.

Experimental Section

Experimental studies on kinetics of intramolecular recombination of randomly generated polymer radicals were performed by pulse radiolysis with spectrophotometric detection.[18−21] Measurements

were made in oxygen-free aqueous solutions, and poly(ethylene oxide) (PEO) was used as the model polymer.

To limit the probability of intermolecular recombination, one has to work using dilute polymer solutions (below the hydrodynamic coil overlap concentration), where, upon irradiation, polymer radicals are almost solely generated by indirect effect. Radiation energy is absorbed by water, resulting in the formation of highly reactive species: hydroxyl radicals, hydrogen atoms, and hydrated electrons (eq 4). Saturating the solution with nitrous oxide removes oxygen (that could interfere in further reaction steps) and doubles the radiation-chemical yield of hydroxyl radicals (eq 5). The latter react with PEO at a diffusion-controlled rate by hydrogen abstraction, producing carbon-centered radicals at random positions along the polymer chains (eq 6). Their subsequent decay by (mostly intermolecular) recombination and disproportionation (eqs 7a and 7b) is the process followed in this study.

$$H_2O \xrightarrow{\text{ionizing radiation}} {}^{\bullet}OH,\ H^{\bullet},\ e^{-}_{aq},\ H_3O^{+},\ H_2O_2 \tag{4}$$

$$N_2O + e^{-}_{aq} + H_2O \longrightarrow {}^{\bullet}OH + OH^{-} + N_2 \tag{5}$$

$$\text{—}CH_2\text{–}CH_2\text{–}O\text{—} + {}^{\bullet}OH \longrightarrow \text{—}CH_2\text{–}\overset{\bullet}{C}H\text{—}O\text{—} + H_2O \tag{6}$$

$$\text{—}CH_2\text{–}\overset{\bullet}{C}H\text{—}O\text{—} + \text{—}CH_2\text{–}\overset{\bullet}{C}H\text{—}O\text{—} \longrightarrow \text{—}CH_2\text{–}\underset{\displaystyle \text{—}CH_2\text{–}CH\text{—}O\text{—}}{\overset{\displaystyle \text{—}CH_2\text{–}CH\text{—}O\text{—}}{CH}}\text{—} \tag{7a}$$

$$\text{—}CH_2\text{–}\overset{\bullet}{C}H\text{—}O\text{—} + \text{—}CH_2\text{–}\overset{\bullet}{C}H\text{—}O\text{—} \longrightarrow \text{—}CH{=}CH\text{—}O\text{—} + \text{—}CH_2\text{–}CH_2\text{–}O\text{—} \tag{7b}$$

Besides the efficient reactivity transfer mechanism (eqs 4−6), using aqueous solutions has also other advantages. The radiation-chemical yield of radicals in water is significantly higher than in most organic solvents, water-derived reactive species are short-lived, and their absorption spectra do not significantly overlap with the spectra of polymer radicals, thus allowing for undisturbed decay kinetics analysis of the latter.

Poly(ethylene oxide) is the polymer of choice for our kinetic studies, since, in contrast to most other water-soluble polymers, irradiation of this compound leads to the formation of only one kind of radicals. This allows to avoid potential problems that may result from a too complex reaction mechanism when many different radicals, of different absorption spectra and reactivity, are present in the system, as has been demonstrated for polyvinylpyrrolidone,[30] poly(vinyl alcohol),[26] poly(vinyl methyl ether),[13,29] poly(*N*-isopropylacrylamide),[31,32] synthetic polyelectrolytes,[27,33,34] etc.

Two standards of PEO (Polymer Laboratories, $M_p = 94$ kDa and $M_p = 276$ kDa, $M_n/M_w < 1.1$) were used to ensure well-defined chain length of relatively narrow distribution. Aqueous solutions of PEO (10 mM of monomer units unless otherwise indicated), saturated with N_2O, were pulse-irradiated in a quartz flow cell with 6 MeV electrons from a linear accelerator (electron path 7 mm, transverse optical path 10 mm). Electron pulses were of 17−500 ns duration, and the dose per pulse could be varied from ca. 10 to 400 Gy (1 Gy = 1 J kg^{-1}). Reactions 4−6 were essentially complete within the duration of the pulse. Subsequently, the decay of PEO radicals was followed by fast spectrophotometry at $\lambda = 270$ nm. To obtain data of reasonable signal-to-noise ratio, each recorded kinetic trace was an average of at least 16 individual shots. Calculations of radical concentrations were based on an extinction coefficient of PEO radicals equal 570 dm^3 mol^{-1} cm^{-1} at $\lambda = 270$ nm,[12] and a small correction has been applied to compensate for the (very low) absorbance of stable, final irradiation products.

Simulation Method. We use a version of the cooperative motion algorithm (CMA)[35−37] developed to simulate single polymer chains.[38] This simulation method has been proved to provide information on the static and dynamic properties of polymer molecules of complex topologies: linear chains, cycles, catenanes,[38] stars,[39] brushes or microgels.[39] In this work we simulate the process of nanogels formation; i.e., the topology of simulated macromolecules changes in time. In the simulations using CMA method a macromolecule is represented by a simplified model of an ensemble of beads located at lattice sites connected by nonbreakable bonds in such a way to represent the macromolecule topology. In such a simplified model one bead represent a segment of the chain (a group of atoms). The systems are considered under the excluded-volume condition, which means that each lattice site can only be occupied by a single molecular element (bead). Each bead is described by a set of numbers defining its position in the chain, in space, connections with other beads of the macromolecule and other properties if needed. The beads are allowed to change their positions on the lattice in a random way so that the molecule is flexible and mobile, observing however the chain continuity condition. Bonds are represented by vectors. The presented results are obtained by simulations on a fcc lattice, where the bonds have length $a = \sqrt{2}$. The possible bond angles are $\alpha = 60°$, 90°, 120°, and 180° with degeneracy $d_\alpha = 2$, 4, and 1, respectively. The coordination number of the lattice is equal to 12; i.e., every monomer has 12 nearest neighbors. Monitoring positions and/or orientations of system elements in time allows to detect the dynamics in such a system. Quantities characterizing the system are calculated only between cooperative rearrangement steps. One time unit corresponds to a number of simulations steps after which an average of one attempt to move each bead was made. A more detailed description of the algorithm used can be found in refs 35−40.

We simulate cross-linking of linear chains by recombination of "radicals" generated on the chain. Generation of the radical on a bead is simulated by ascribing to it a property of interacting with other "radicals" while its other properties remain the same. In each simulation cycle a new linear chain in a random conformation was generated on the lattice. A given number of radicals was generated on the chain simultaneously at random or fixed positions at time $t = 0$. In the case of random generation, the radicals are not allowed to be generated at a distance smaller than 5 beads from one another. The chain is then allowed to move, and the distances between the radicals are monitored once per time unit. If some two radicals get in close contact, i.e., the distance between them becomes equal to the bond length a, the radicals are allowed to "recombine", forming a new bond between the beads on which they were located or to "disproportionate" (they disappear, i.e., the two beads lose the property of being the "radicals") with some probabilities. The decay of radicals and other chain properties are monitored in appropriate time intervals and averaged over subsequent simulation cycles, i.e., on the number of chains. The simulation of this type is efficient and allows to average the properties of chains consisting of a large number of beads (e.g., 100 chains of length $N = 640$) within the time period by factor 10^6 longer than the relaxation time of a single bead, using a personal computer. The chain length was $N = 20$, 40, 80, 160, 320, or 640, in some cases up to 2560.

The following parameters were calculated at appropriate time intervals: average number of radicals on the chain Z, end-to-end vector of the chain $\mathbf{R}$ and of the subchain (chain segment) at the end of which the radicals were generated $\mathbf{Rr}$ (radical-to-radical vector), the single bond autocorrelation function

$$\rho_{b(t)} = \frac{1}{Nn}\sum_{n}\sum_{i}^{N} b_{i(t)}b_{i(0)} \tag{8}$$

where b_i are unit vectors representing bond orientation and n is the number of simulated chains, and the end-to-end vector autocorrelation function

$$\rho_{(t)} = \frac{1}{n}\sum_{i=1}^{n} \mathbf{R}_{i(0)}\mathbf{R}_{i(t)} \tag{9}$$

where $\mathbf{R}_{(0)}$ and $\mathbf{R}_{(t)}$ are end-to-end vectors at time $t = 0$ and t, respectively.

The averaging was performed over the ensemble of n successively generated chains. In most cases data for at least 400 chains were averaged. For the longest chains we performed simulations until at least 400 averaging per radical pair could be made.

The above correlation functions have been used to determine corresponding relaxation times τ by fitting a sum of stretched exponential (KWW) functions

$$r_{\mathrm{fit}}(t) = \sum_i A_i \exp\left[-\left(\frac{t}{\tau_i}\right)^{\beta_i}\right] \tag{10}$$

where the number of components i was 1 or 2. The same function was used to fit the averaged time dependence of radical number per chain Z. It was shown that this representation is equivalent to dispersive kinetics (eq 1) for the first-order reactions with $\beta = \alpha$. Fitting the simulation results, we took into account first of all the central part of the curve (e.g., in the case of radical decay the range in which 10−90% radicals recombined) because the initial and terminal parts are not accessible experimentally or the errors can be very important. Also in the simulations the number of recombinations being averaged for short and long times is small, which results in significant relative error of the obtained results.

Results and Discussion

Simulations of the Decay of Radicals Generated at Fixed Distances. Recombination of radicals on the chain requires that two parts of the chain came into close contact. It is therefore controlled by dynamics of chain segments. The bigger is the distance between the radicals in space and measured along the chain, the slower is their recombination. In contrast to recombination of radicals on small molecules, the radicals on polymer chain cannot diffuse apart more than it is allowed by the chain continuity condition, and their average distribution in space is different. The average distance between them and recombination probability are determined by the chain length and the chain conformation statistics. Therefore, if the radicals are generated close in space but on distant chain segments, the situation is different than when they are close to each other on the chain. To elucidate the effect of radical positions on the chain, simulations of recombination of radicals located at fixed positions on chains of different length have been carried out.

The radicals were generated on a chain of N beads at fixed sites $r_1 = (N - N_R)/2 + 1$ and $r_2 = N - (N - N_R)/2 = (N + N_R)/2$, i.e., at the ends of a central subchain $r_1...r_2$ of N_R beads. The distance between the radicals in space **Rr** is therefore equal to the end-to-end vector of the subchain N_R; i.e., it has a typical Gaussian distribution.

Scheme 1. Chain Model for Simulations of the Decay of Two Radicals r_1 and r_2 Generated at Fixed Distances

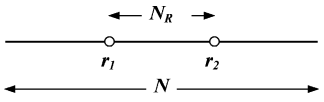

In Figure 1, the time dependence of radical decay for the two subchains $N_R = 20$ and $N_R = 80$ being parts of chains of different length N is presented. It can be seen that the decay kinetics of the radicals separated by a subchain of the same length depend on the total chain length and the decay is slower for higher N as could be expected. The radical recombination is slowed down by ca. 1 order of magnitude already for chains about twice as long as the inter-radical distance, and the effect of farther increase of the total chain length is negligible. A relatively strong effect of only two additional beads added at the ends of the chain (cases $N = 20$ and $N = 22$) is due to the effect of steric hindrance.

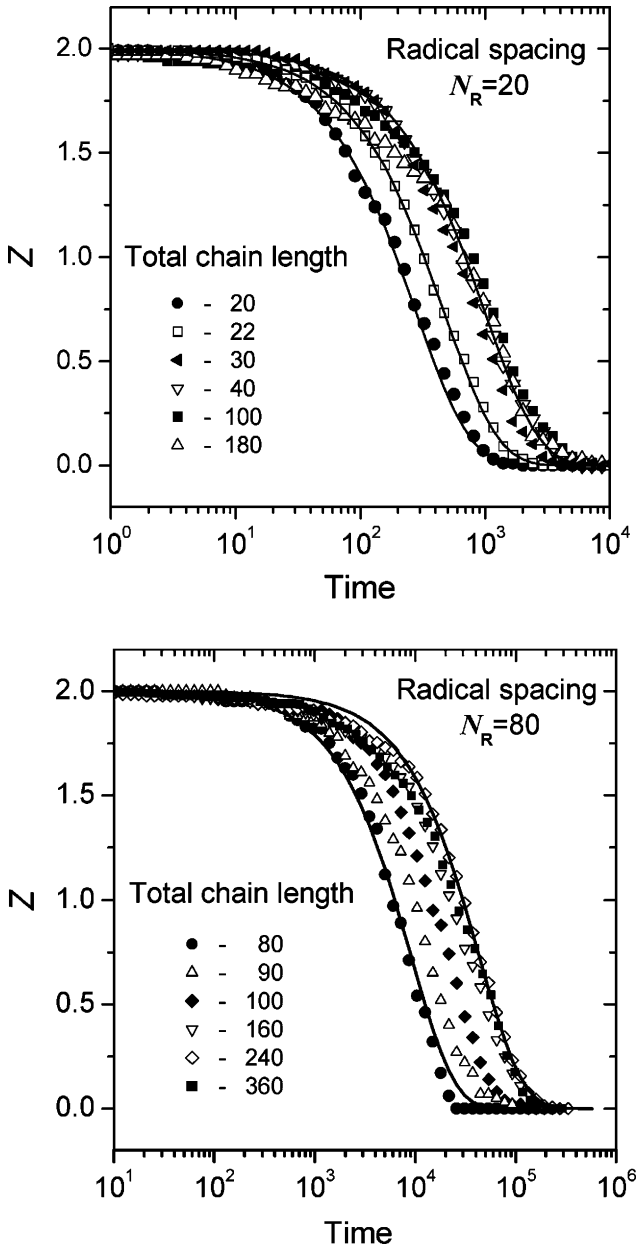

Figure 1. Decay of radicals generated at the ends of subchains of $N_R = 20$ and $N_R = 80$ of chains of various total lengths N.

It is interesting to note that the radical decay on chains not much longer than the distance between the radicals N_R can be fitted quite well using a simple exponential function (solid lines in Figure 1, according to eq 10, $\beta = 1$) over entire time range; i.e., it follows first-order kinetics. In the case of long chains the exponential decay is also observed for most of the time, but the initial decay is slightly faster. It can be explained taking into account that the radicals generated close to each other in space, i.e., on a subchain of a small **Rr**, cannot diffuse apart so fast on long chains because it requires rearrangement not only of the subchain but also of adjacent parts of the chain of comparable length. Thus, recombination probability is somewhat higher.

Generation of radicals separated by fixed N_R means that they are generated at various distances in space. We performed also some simulations of the reverse case: the first radical was generated at the same position $\mathbf{r}_1$ with respect to the chain end

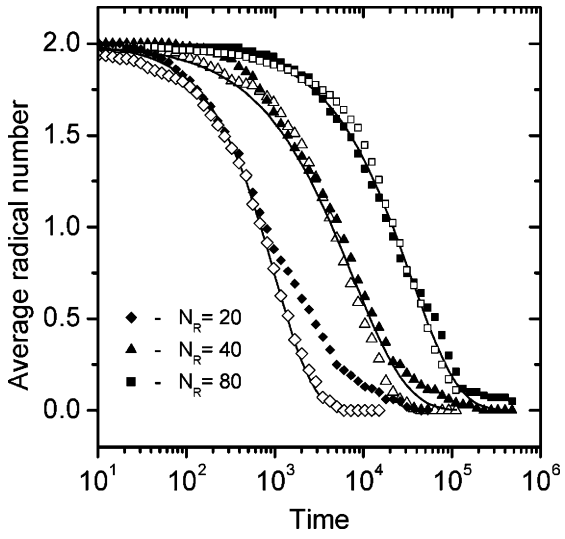

Figure 2. Recombination of radicals generated at fixed distances in space (full symbols) and along the chain (empty symbols) (see text for details). The lines show fits using stretched exponentials with $\beta = 0.72$.

(as in the corresponding previous simulations), but the second was generated at a bead being in a fixed distance in space from the first one, regardless of its position on the chain. Thus, the initial distance in space was constant but the number of beads between the generated radicals varied, depending on the initial chain conformation. The relationship between the two cases is illustrated in Figure 2. The full symbols correspond to fixed N_R = 20, 40, and 80 while the empty symbols correspond to generation of radicals at a fixed distance in space, equal to the average end-to-end distance of the chains $N = 20$, 40, and 80. The total chain length is equal to $4N_R$ in all these simulations.

One can see that in the recombination half-time is similar. In the second case, however, the decay can be better fitted using the stretched exponential (eq 10 with $\beta = 0.72$). Some systematic discrepancies are observed for short and long times. The average chain conformations in the two cases differ slightly because it was not possible to generate the second radical on the chains on which for all the beads their distance to $\mathbf{r}_1$ was smaller than **Rr**. Such chains were not taken into account, but it means that the average radius of gyration of the ensemble of chains in these simulations was somewhat bigger as compared with an ensemble in the simulations in which N_R was fixed.

An important point is that the radicals generated on equivalent distances along the chain and in space have similar recombination half-times and only slightly different recombination kinetics; thus, we can use the first, more universal and more convenient generation method to study an effect of various parameters which can influence the recombination kinetics.

It can be expected that the recombination half time of a pair of radicals on a polymer chain is related to the relaxation time of the subchain between them. The relaxation time being a simple parameter characterizing the chain dynamics is usually determined using the end-to-end vector autocorrelation function ρ_R (eq 9). The relaxation of a subchain is however not simply related to the relaxation time of an individual chain of the same length. Calculations using Rouse and reptation models[41,42] and experiments on block copolymers[40] have shown that the relaxation of the segment within a long chain is much slower than the relaxation of the free chain of the same length. There is however some discrepancy between the calculated and experimental results as discussed in ref 40.

Figure 3a presents the comparison of the end-to-end autocorrelation function ρ_{R20} of the central chain segment of 20 beads

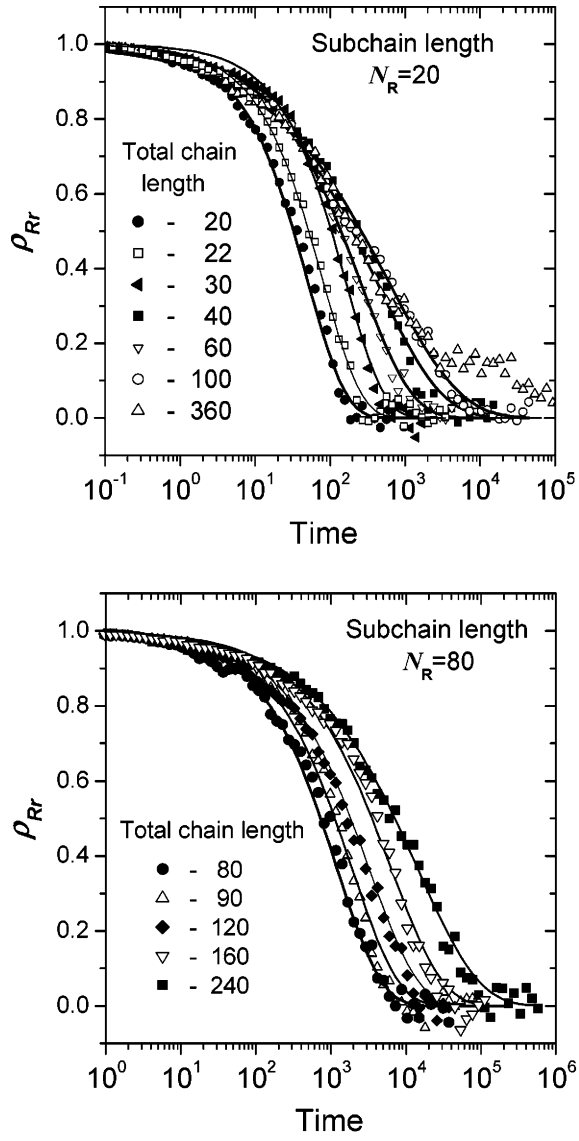

Figure 3. End-to-end autocorrelation functions ρ_{Rr} of the central chain segment of $N_R = 20$ and $N_R = 80$ beads in the chains of different lengths.

in the chains of different lengths, from $N_R = 20$ to 360, while in Figure 3b analogous data on ρ_{R80}, for $N_R = 80-240$ are shown.

It can be seen that in the case of chains more than twice longer than N_R for short times the relaxation process is little dependent on N. By contrast, the total chain length has a strong influence on the long time relaxation. In other words, partial reorientation of the subchain end-to-end vector depends mostly on local movements, while complete relaxation is a slow process controlled by the total chain relaxation, even if the chain is 18 times longer than the segment in question.

In Figure 4, dependences of $t_{1/2}$ and τ on the total chain length are compared for $N_R = 20$ and 80.

In the case of radicals on a subchain not much shorter than the total chain length the decay half-time and the **Rr** relaxation time are significantly different, but for the same subchain on the long chains the two parameters are of the same order.

It is also interesting to compare recombination of radicals separated by different number of chain segments on a long chain. As discussed later on, comparing decay kinetics for longer and longer subchains, we can get an insight into the situation at different stages of recombination of multiple radicals randomly

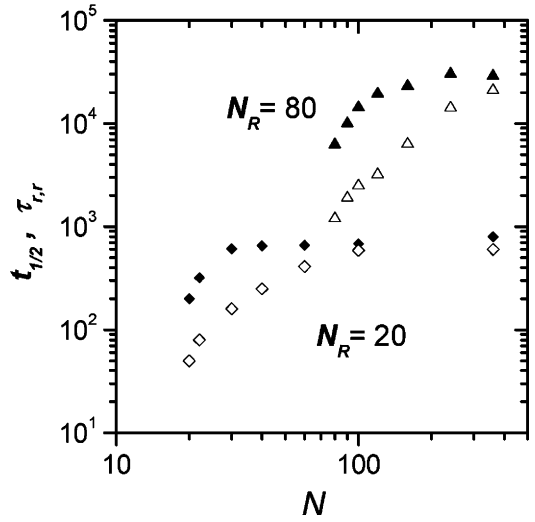

Figure 4. Dependence of $t_{1/2}$ (full symbols) and τ (open symbols) of the subchains $N_R = 20$ (diamonds) and $N_R = 80$ (triangles) on the total chain length.

spaced on one chain. Results of the simulation of such model cases are presented in Figure 5.

For small N_R the first, dominating relaxation process (of lower τ) has bigger β coefficient (equal to 0.63). The second, slower relaxation process is more distributed, $\beta = 0.4$. Its contribution falls down with increasing N_R, and for $N_R = 80$ a single stretched exponential gives a reasonable fit. It should be noted that if the fit is made using the sum of two stretched exponentials there is no simple relationship between the two relaxation times and a decay half-time.

The kinetics of radical recombination corresponding to this case is shown in Figure 5b. For comparison, the corresponding subchain end-to-end relaxations ρ_{Rr} are also shown as solid lines. It can be seen that the radical decay is generally slower (note that an agreement between the line and points for $N_R = 40$ is accidental). In these simulations the radical decay can be described by simple exponentials for all N_R. It can also be seen that (comparing with ρ_{Rr}) the N_R dependence of $t_{1/2}$ levels off for much bigger N_R, close to N. An anomalous, faster decay of radicals on the ends of the chain is again due to higher mobility of chain ends and smaller steric hindrance in this case (cf. discussion of the results shown in Figure 1).

Comparing Figures 1, 3, and 4, one can conclude that although there is a qualitative relationship between the **Rr** relaxation and radical decay dependence on the total chain length, the two processes have different dynamics, especially for short segments on long chains. Recombination remains a local process and its dependence on the total chain length levels off for chains about twice as long as the segment length. Moreover, it is in all cases described by the simple exponential law. By contrast, the end-to-end vector relaxation of the subchain N_R (as measured by its end-to-end vector autocorrelation function) not only depends more strongly on the total chain length, but also its relaxation becomes broader and broader as the total chain length increases. For $N > 3N_R$ it can no longer be described by a single stretched exponential, and a sum of at least two is necessary (see Figure 5b).

Influence of Loops. As a result of recombination of radicals loops are formed on the chain. An influence of such loops between radicals on their recombination kinetics can be related to two effects: (i) a loop between the radicals is a sort of obstacle, making their coming in contact less likely, and (ii) the distance between them, measured along the chain contour

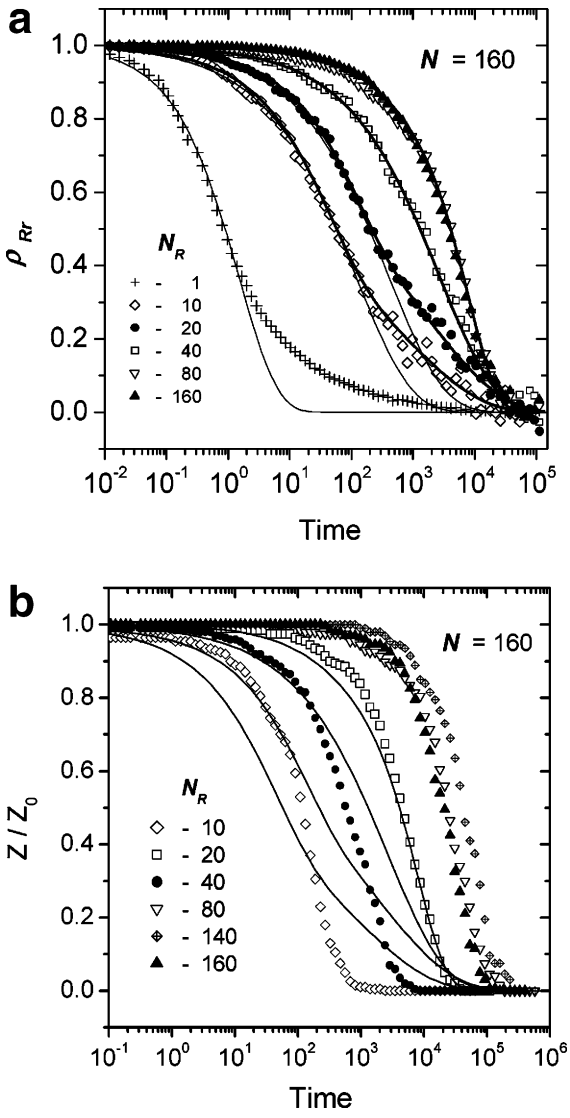

Figure 5. End-to-end relaxation ρ_{Rr} (a) and normalized radical decay (b) for central subchains of different N_R (given in the legend) on chains of $N = 160$. In (a) solid lines represent fits using stretched exponential function (thin lines) or a sum of two stretched exponentials (thick lines). The solid lines in (b) represent the same fits to ρ_{Rr} as in (a) 10, 20, 40, and 80 compared with the decay of radicals generated on the ends of the same subchains (symbols).

is reduced. The average distance between the radicals in space is also reduced. We performed simulation of radical recombination on model chains on which a loop was formed in the middle, between a pair of radicals generated at fixed distances N_R (Scheme 2). In this case N_R is the number of beads of the shortest $r_1...r_2$ subchain, i.e., not including the loop. Figure 6 shows decays of pairs of radicals of $N_R = 40$ on chains on which loops of $N_L = 10$, 20, and 80 beads were formed and the decay of pairs of radicals of $N_R = 20$ with a loop of $N_L = 20$. The decays for linear subchains of $N_R = 20$ and 40 are also shown for comparison. In all cases the distances between the radical and the chain ends are the same, equal to 40; i.e., as shown before, the recombination kinetics is close to that on infinite chain. One can see that the recombination on chains with the loops is slower ($t_{1/2}$ increases ca. 2 times, but the effect of the loop length is negligible).

It should however be noted that the recombination on the chains with loops is much faster as compared with the case of the same total number of beads between the radicals $N_R + N_L$

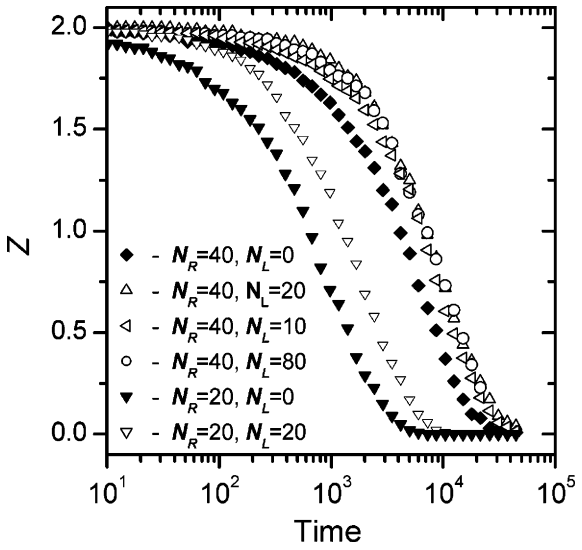

Figure 6. Comparison of radical decays on linear chains (full symbols) and on chains with a loop of different length N_L (open symbols) (see text for details).

Scheme 2. Chain Models Used in Simulations Testing the Influence of Loops on Recombination Kinetics

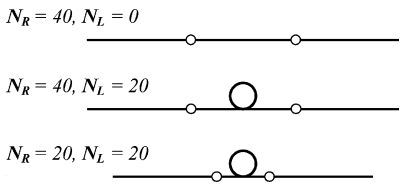

but without the loop (compare the case $N_R = 20$, $N_L = 20$ and $N_R = 40$, $N_L = 0$ in Figure 6).

Thus, in the case of recombination of multiple radicals on long chains the influence of loops formation has indeed a twofold effect on the recombination kinetics. The steric effect of loops compensates to some extent the decrease of the distances between the radicals. The latter is much stronger for big loops on short subchains, but it should be noted that such a case is rather unlikely because it occurs when a radical recombines with the neighbor to which the initial distance was considerably bigger than that to the other neighbor.

Simulations of the Decay of Radicals Generated at Random Positions. Typical decays of the radicals in recombination of two and eight radicals generated at random positions on chains of different length are shown in Figure 7. Similar as in the case of radicals generated at fixed positions, the half-life of radicals increases with increasing chain length (Figure 8). However, the time dependence is generally broader (compare Figures 1, 2, 5, and 7), and a stretched exponential (eq 10 with $i = 1$) must be used to fit the data. Moreover, the β parameter decreases with increasing chain length from 0.7 to 0.48. Taking into account the results obtained for fixed distances between the radicals, we can relate this effect to the distribution of the distances between the radicals.

Decay half-times for various numbers of radicals per chain are collected in Figure 8.

Comparing the case of 2 and 8 radicals on the chains of the same length, one can see that the decay half time is by ca. 2 orders of magnitude smaller in the later case (due to smaller average distance between the radicals) but the time dependence becomes weaker. The initial distribution of distances between neighboring radicals (in bond units along the chain contour) is shown in Figure 9. It can be seen that on long chains it is close

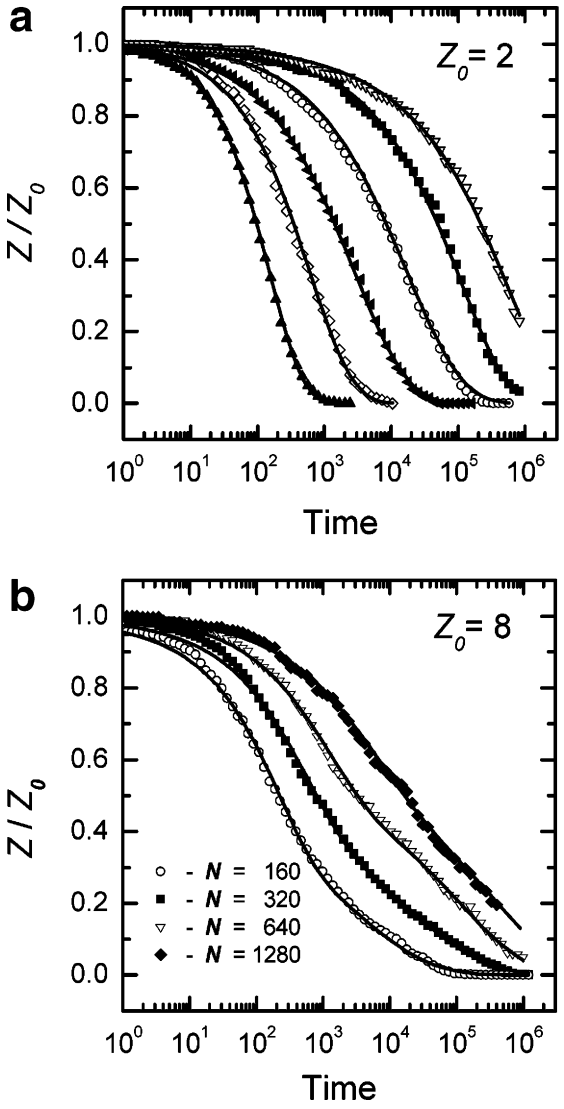

Figure 7. Recombination kinetics of randomly generated two (a) and eight (b) radicals on chains of various length N: ▲, 20; ◇, 40; ▲, 80; ○, 160; ■, 320; ▽, 640.

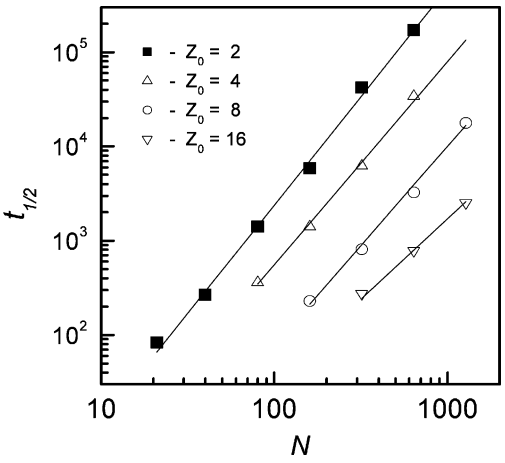

Figure 8. Half-lives of radical recombination for randomly generated radicals ($Z_0 = 2$, 4, 8, 16) as a function of chain length. Slopes are equal to 2.3, 2.15, 2.1, and 1.7, respectively.

to exponential distribution. For short chains it becomes close to triangular—there is a cutoff at the chain length, and the contribution of long distances is decreased. This is the main reason for the changing time dependence, especially for $Z_0 =$

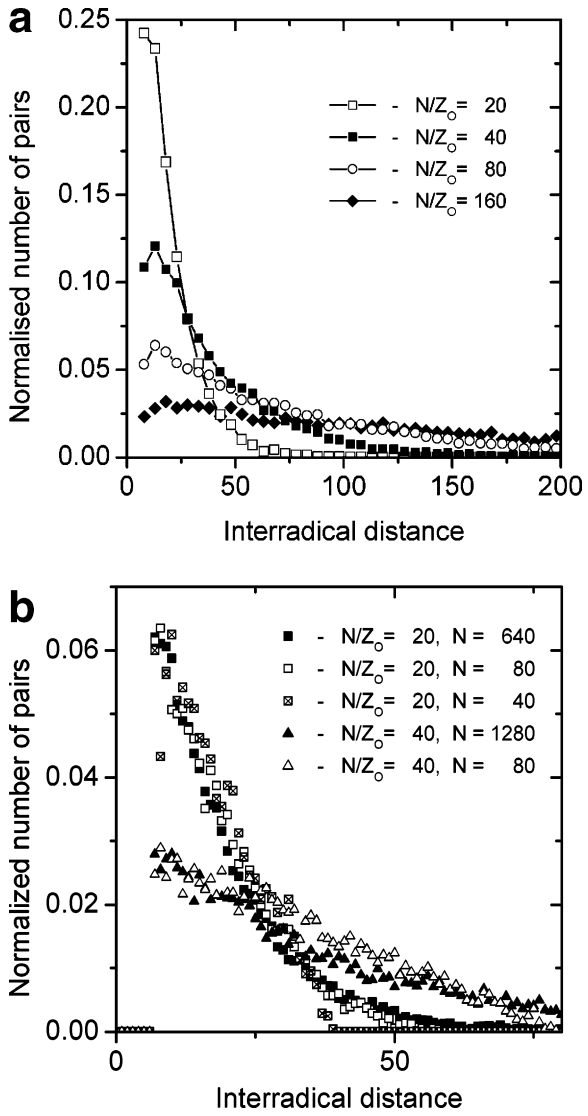

Figure 9. Initial distribution of distances between neighboring radicals (in bond units, measured along the chain contour) for different radical densities on long chains ($N = 1280$) (a) and for two N/Z_0 on chains of different length (indicated in the legend) (b).

2. For fixed N_R the β parameter in stretched exponential fit functions was constant, equal to 1, while in the case of random radical generation it increases with increasing N.

If more than two radicals are generated on a chain, the recombination process becomes more complicated because a given radical can in principle recombine with any other. The simulation results show, however, that the recombination with the nearest neighbor is strongly favored, in agreement with the results presented in the previous section (decay half-times and thus probabilities of recombination strongly depend on the distance between the radicals).

After recombination of some pairs the distances between remaining free radicals are bigger than their distances to the nearest neighbors at the beginning. The process becomes even more complex due to formation of loops. Successive recombination stages are schematically depicted in Scheme 3, and snapshots of the simulated chain are shown in Figure 10.

The illustrated mechanism leads to a complicated time dependence which can be in the first approximation fitted by a sum of two stretched exponentials. The first one (of smaller τ) can be considered as representing the nearest-neighbor recombination and the second one as representing the successive

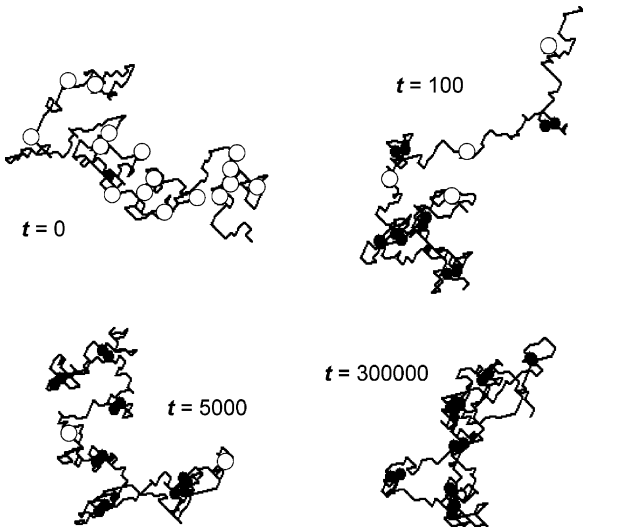

Figure 10. Screenshots illustrating subsequent stages of radical recombination and nanogel formation in the simulation. Projections of chain of $N = 160$ and $Z_0 = 16$ after indicated time are shown. Open circles denote free radicals, and filled circles are the locations of radicals that have already recombined.

Scheme 3. Succesive Recombination Stages

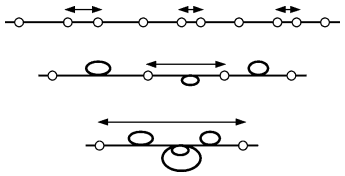

recombinations of the remaining radicals. For a constant Z_0 it seems reasonable to assume that the relative contributions of the two processes are independent of chain length. It leads to consistent sets of other parameters, and such fits are shown in Figure 7b as solid lines. The parameters used in fittings radical decays for various Z_0 are collected in Figure 11. These plots allow an approximate prediction of radical decay for different N by using eq 10 and interpolated or extrapolated values of the parameters.

Figure 12 shows the kinetics of recombination in the case of various numbers of radicals (Z_0) generated on the chain of the same length. Z_0 has a strong influence both on $t_{1/2}$ and on the time dependence of recombination. It is clearly seen especially after normalization (Figure 12b).

The main reason for these differences is the decrease of an initial average distance between the radicals with increasing Z_0. Figure 13 presents the dependence of $t_{1/2}$ on N/Z_0 showing similar scaling behavior as obeyed for pairs of radicals generated on chains of increasing length (Figure 8), which is analogous to increasing N/Z_0.

A comparison of radical decays on chains of various length, where the ratio of the initial number of radicals to the chain length is constant for all the data series ($N/Z_0 = 1/20$ and $1/80$), is shown in Figure 14. It can be seen that despite different chain lengths and numbers of radicals, the half-lives of radicals located, on average, at similar distances are close to each other. Moreover, also the time dependence is at the beginning quite similar (except for smallest N) up to $Z/Z_0 \cong 1/e$, while for longer times it depends strongly on the chain length. The longer is the chain the slower is the terminal decay, and it starts to slow down earlier on long chains. This effect can be understood if we take into account that only at first the average distance between the radicals is the same for short and long chains. After recombina-

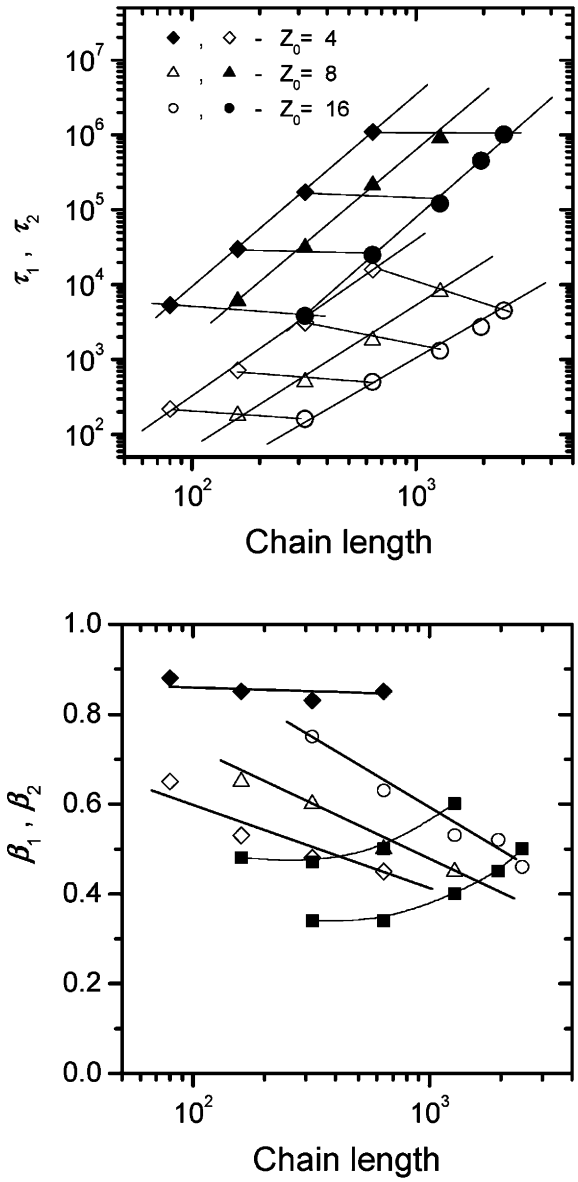

Figure 11. Parameters τ_1, τ_2 and β_1, β_2 obtained by fitting radical decays plotted vs chain length. Contributions of the first (faster) process are 0.65, 0.60, and 0.55 for 4, 8, and 16 radicals per chain, respectively. Empty symbols: τ_1, β_1; full symbols: τ_2, β_2. Lines are guides for the eyes.

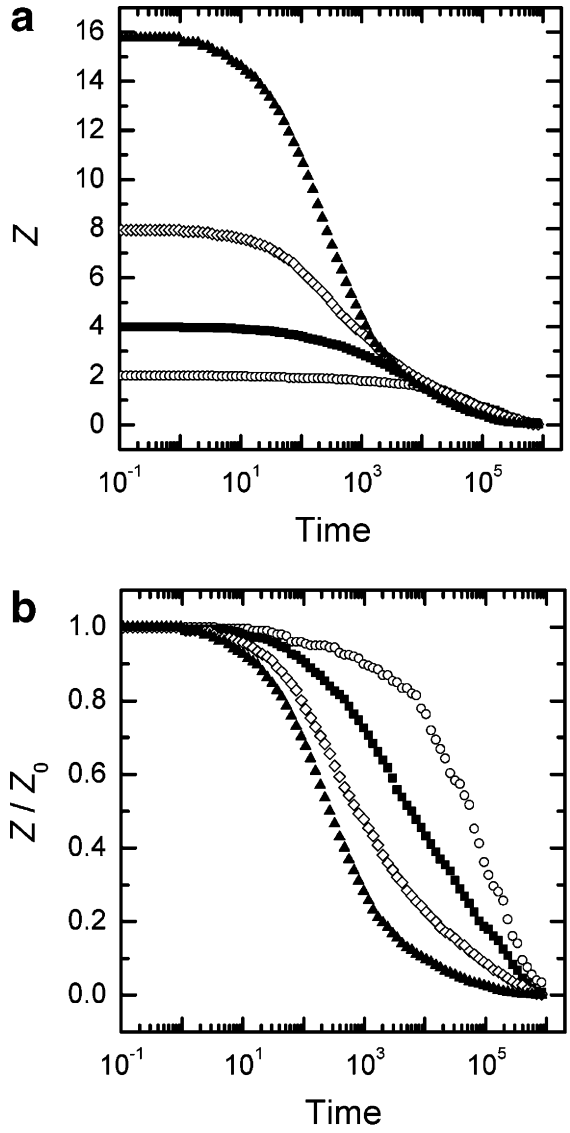

Figure 12. Recombination kinetics of radicals for $N = 320$ and various initial number of radicals per chain: ○, 2; ■, 4; ◇, 8; ▲, 16. (a) Original data and (b) normalized data.

tion of some of the radicals those remaining on short chains are still relatively close to each other (the distance between them is limited by the chain length), while those remaining on long chains are much more distant from each other. In other words, the rate constant decreases significantly slower in time for long chains.

In Figure 15 results of simulations of radical decay by recombination (molecule topology changing in time, formation of loops) and disproportionation (the chain topology does not change) are compared.

Kinetics of recombination and of disproportionation, under identical conditions, shows practically no difference, with equal half-lives. This is in evident contrast with the hypothesis that the formation of internal cross-links causes a considerable stiffening of the structure and consequent retardation of radical−radical reactions. In view of the results of simulations of the effect of loop formation, discussed in the former section, it means that in the case of random radical generation the effect of steric hindrance and of decreasing the effective distance between the radicals due to cross-linking nearly compensate.

Influence of Radical Transfer Reactions. In the above-described simulations we assumed that once a radical is generated, it is located at a fixed position along the chain until it reacts with another radical. In real systems, this assumption is not necessarily fulfilled (see the discussion of experimental data below). Radicals may change their positions by abstracting hydrogen atoms from other locations along the chain. The hydrogen atom is transferred to the "old" position of the radical (and the radical site at this location disappears), while a new radical is formed at the position from where the hydrogen atom was abstracted.

Radical transfer neither changes the number of radicals along the chain nor creates a cross-link. However, it is not negligible for the kinetics of radical recombination, since it changes the distribution of distances between the radicals along the chain. It is clear from the simulations that the distribution of these distances plays a key role in determining the recombination rate. In an undisturbed system, at late recombination stages large distances between the radicals dominate. Reshuffling the distance distribution introduces some closely located radical

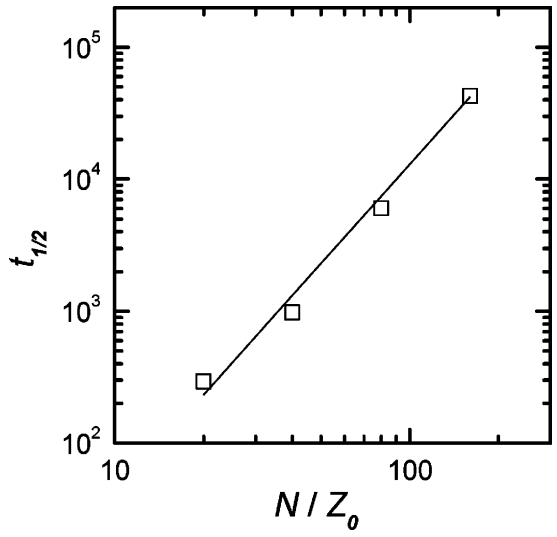

Figure 13. Recombination half-life of radicals randomly generated at an $N = 320$ chain as a function of initial radical density on the chain N/Z_0.

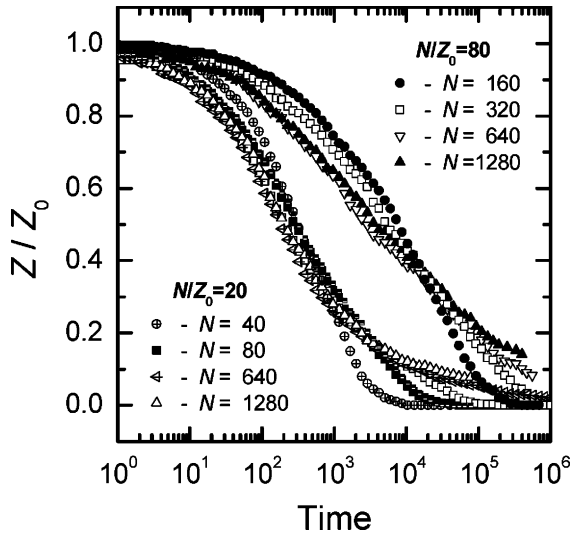

Figure 14. Radical decays for $N/Z_0 = 80$ and $N/Z_0 = 20$ and different chain lengths.

pairs, and this should lead to increased recombination rate when compared to systems where this effect is absent.

To demonstrate the potential influence of radical transfer on the kinetics of recombination, we performed simulations according to a modified algorithm that allowed incorporating this process.

Exemplary results for one pair of radicals randomly generated on a chain of 320 beads are presented in Figure 16. The data series correspond to various radical transfer probabilities, from 0 to 0.1.

It is evident that radical transfer, even slow, has a significant influence on the kinetics of recombination because the transfers can significantly reduce big initial distances between radicals thus accelerating recombination. This influence is small at short times (the distribution is not significantly modified after few transfers), but at longer time scales the decay half-time is decreased with increasing radical transfer probability (the more the longer is the chain). Dispersive character of recombination kinetics is less pronounced (β exponent increases).

Comparison with Pulse Radiolysis Experiments. The main aim of performing the above-described simulations is to deepen our understanding of intramolecular radical recombination in

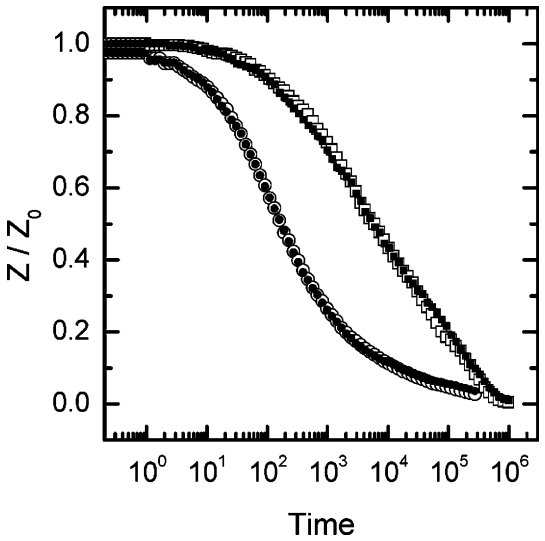

Figure 15. Kinetics of decay of radicals by pure recombination (open symbols) and pure disproportionation (corresponding filled symbols) simulated for two cases. □: $N = 320$, $Z_0 = 4$; ○: $N = 640$, $Z_0 = 32$.

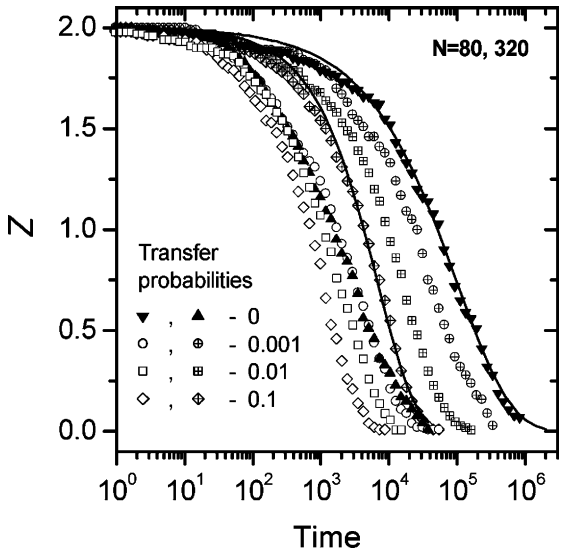

Figure 16. Influence of radical transfer along the chain on radical decay on chains $N = 80$ (open symbols) and 320 (crossed symbols). The data sets correspond to various transfer probabilities (from 0 to 0.1) indicated on the figure. Lines for $N = 320$ are to guide the eyes.

real systems. Therefore, it is important to see how simulation results compare with experimental data; thus, we performed pulse radiolysis experiments on PEO standards.

Certainly, such a comparison can only be made for simulations which correspond to a real situation and not to purposely simplified model cases. In particular, in experiments upon pulse irradiation of solution the radicals are generated randomly along the chain; thus, the comparison can only be made to simulations with random radical generation.

To compare results of simulations with experiment, we must adopt suitable scaling of Monte Carlo time and N. Experimental data on poly(ethylene oxide) were compared with simulations which were performed assuming that two monomer units correspond to one MC segment (cf. ref 43). To obtain proper time scaling, MC time unit is assumed to be equivalent to 7×10^{-9} s. Such time scaling is justified not only by the correspondence of the experimental and simulation results but also by the correspondence of the orientation relaxation times. From

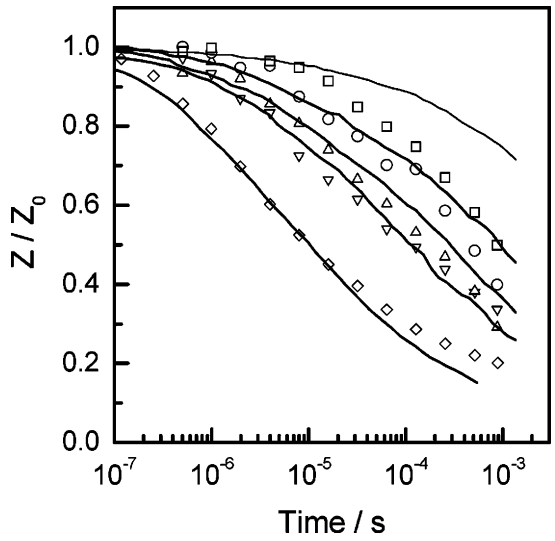

Figure 17. Comparison of experimental and simulation data on the kinetics of recombination. Series of points represent experimental data for 10 mM PEO monomer units, $M_p = 94$ kDa (2136 monomer units), for various average initial numbers of radicals per chain (Z_0): ◇, 21.0; ▽, 7.2; △, 6.0; ○, 4.1; □, 2.7. Simulation data (random radical generation) for $N = 1068$ shown as curves, from bottom to the top $Z_0 = 20$, 8, 6, 4, and 2.

the simulations we can also obtain the relaxation time of the MC segment equal to 2 MC time units. The relaxation time for a Kuhn segment of PEO in water (six bonds), determined by molecular dynamics simulations, is ca. 3×10^{-10} s and for a C−C bond ca. 1×10^{-11} s,[43] in agreement with NMR data (1.8×10^{-11} s[44]). Thus, taking into account that only some contacts between beads in the simulations correspond to configuration for which the radicals can recombine, we can conclude that such time scaling is reasonable.

Figure 17 illustrates the comparison between experimental data on the recombination of PEO radicals and the corresponding simulation results. In general, reasonable agreement is observed, except for the data at the highest N/Z_0 values, for which final part of recombination is much faster in experiments.

The potential discrepancies between the data from simulation and experiment can originate from differences in radical generation and from side reactions taking place in the experiments.

In the simulations, a fixed number of radicals is generated on each chain, while in reality there is a distribution of numbers of radicals generated on macromolecules. Thus, even if the initial average distance between the radicals is similar for the compared simulation and experimental data sets, the radical distance distribution in experiment might be broader, and this could lead to a somewhat broader kinetic curve of radical decay.

Some additional correction should be made taking into account that in the simulations an even number of radicals per chain is assumed. In the real system we generate odd and even numbers of radicals; thus, some of them cannot recombine by intrachain recombination.

In principle, a further difference between the simulation model and the real system may be the distribution of chain length. In simulations of a given N, all generated chains are of identical length, which is not the case in typical polymer samples. However, to avoid this problem, in experiments we have used PEO standards of very narrow molecular weight distribution, and therefore this effect is negligible.

The second kind of sources of potential discrepancies between the simulation and experimental data is related to the presence of side reactions in the experiments. Two main side processes should be taken into consideration: radical transfer and intermolecular recombination (and/or disproportionation) of radicals.

To our knowledge, radical transfer reaction in the sense described above has not yet been studied for PEO. It would be actually difficult to follow, since all the H atoms and all the radical positions in this polymer are equivalent. H-abstraction and shifting of radical sites were, however, evidenced for some other simple water-soluble polymers, like poly(vinyl alcohol),[45] poly(acrylic acid),[27] and poly(methacrylic acid),[34] and thus one may infer that such radical transfer reactions take place also in the case of PEO. In the above-mentioned studies there were no indications of a movement of the radicals along the chain, i.e., by an 1,2-H shift between the neighboring carbon atoms. It is rather believed that the H-abstraction takes place over some distance, when a radical-bearing segment comes to proximity in space with some other segment that may be quite distant along the chain. This corresponds to the process discussed and simulated above. In all the studied cases the process was occurring at a moderate rate, with the rate constant at room temperature being on the order of $150-500$ s^{-1}. These data may be used for estimation of an average "waiting time" for an H-transfer, which is a few milliseconds. It is evident that an H-abstraction, in contrast to radical recombination, is not a diffusion-controlled process; i.e., it does not occur at every encounter of a radical site with other chain segment, but rather takes place with some, relatively low, probability.

Taking this into account, this side reaction is not expected to interfere with intramolecular radical recombination at short time, but it may play a role at the later stages by redistributing the distances between the radicals, which is clearly evidenced by simulation with radical transfer (see above). Therefore, we expect that at long time (i.e., mainly for systems of high initial N/Z_0 ratio) the experimentally observed final decay stages would proceed faster than in regular, radical-transfer free simulation.

In simulation of intramolecular radical recombination we study single, isolated chains. In experiments this condition can only partially be met. The choice of experimental conditions is a matter of compromise between the necessity of having the chains separated (and possibly far) from each other and of keeping the concentration at a level high enough to obtain a reasonable signal. At very low polymer concentrations, self-combination of OH radicals ($2k = 1.1 \times 10^{10}$ dm^3 mol^{-1} s^{-1} [46]) competes efficiently with OH−polymer reaction (6), a significant fraction of OH radicals is "lost", and the number of polymer radicals is low.

For the PEO samples used in this study ($M_p = 94$ kDa, $R_g = 24$ nm as determined by static laser light-scattering, and $M_p = 276$ kDa, $R_g = 42$ nm), the coil overlap concentrations (calculated as $c^* = 3M/4\pi N_A R_g^3$,[47]) are equal to 61 and 34 mM, respectively. Thus, on average, the coils are separated from each other, but the distances are not large compared to the coil dimensions. Therefore, an influence of intermolecular recombination (a slower, but potentially efficient, reaction) may be expected to show up at long reaction times. Since intra- and intermolecular recombination are parallel processes, their rates sum up; thus, at long time scales we may anticipate the radical decay in experiment to be faster than in single-chain simulation.

From our simulations we get also mean-square displacement of the center of mass of the chain. Comparing square roots of these values at the time equal to $t_{1/2}$ with R_g, we find that they are of the same order. It means that it is quite likely that at the last stage of recombination some of the neighboring coils overlap

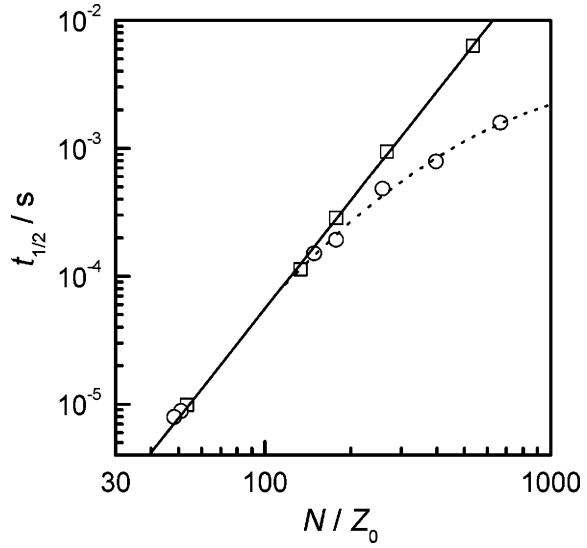

Figure 18. Dependence of recombination half-life on the average distance between the radicals, $N = 1068$: □, simulation with random radical generation; ○, experiment. Dotted line is to guide the eyes.

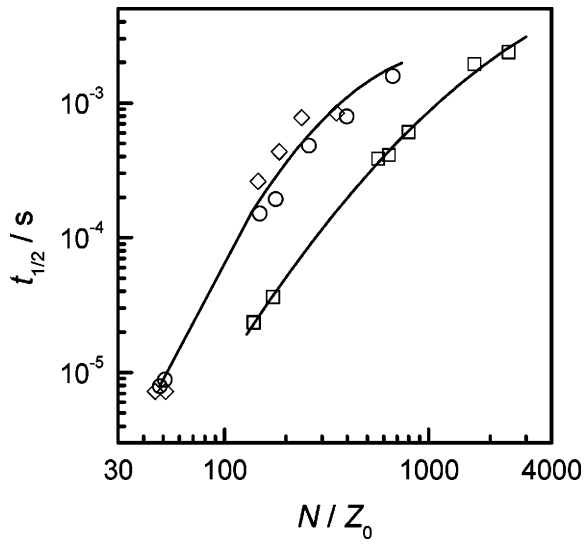

Figure 19. Dependence of recombination half-life on the average distance between the radicals. Experimental data for (○) 10 mM, 94 kDa; (◇) 10 mM, 276 kDa; and (□) 50 mM, 276 kDa.

and interchain recombination can more and more efficiently compete with intrachain one.

The two effects described above seem to be the reasons for discrepancies between simulation and experimental data observed for two highest N/Z_0 values (slowest decays) in Figure 17. This can be also illustrated by comparing the half-life dependence on the N/Z_0 ratio for simulations and experiments (Figure 18). While for low N/Z_0 the shape of dependence is similar, at high N/Z_0 the experimental data start to deviate from the straight line dependence, indicating acceleration of radical recombination, most probably due to H-transfer and to the onset of influence of intermolecular recombination.

The influence of intermolecular recombination can also followed by comparing the data for various experimental conditions, in particular for different polymer concentrations (Figure 19).

While the two data series for 10 mM concentration of 94 and 276 kDa PEO samples nearly converge, the data obtained at 50 mM of 276 kDa PEO (i.e., at a concentration higher than the coil overlap concentration of 34 mM) are clearly different—the decay is faster, and the dependence on N/Z_0 is somewhat less pronounced. This again indicates significant contribution of intermolecular recombination. Indeed, this concentration exceeds the critical concentration.

A further indication that under our experimental conditions, in particular in 50 mM PEO solutions, intermolecular recombination may play an important role is a noticeable increase in average molecular weight observed for single-pulse-irradiated PEO already at a concentration of 32 mM.[48]

Other potentially interfering processes, like first-order decay of radicals by transfer of a radical back to water or by reaction with impurities, are very unlikely to occur with significant yields at the time scales of our observations. Besides the fact that hydrogen abstraction from water molecule by a polymer radical is thermodynamically very unfavorable, many observations indicate that in oxygen-free aqueous systems, where radiation-generated polymer radicals are unable to recombine or disproportionate (because of Coulombic repulsion), the radical lifetime at room temperature extends to minutes or even hours,[27,33,34,49,50] thus indicating the lack of other efficient mechanisms of radical decay.

At the end we would like to address the question of suitability of eqs 2 and 3 for description of intramolecular recombination kinetics. In the analysis of single pair recombination (see above), the stretched exponential, being equivalent to eq 1 with first-order rate coefficient k, seems to be both effective and rational, since each recombination event is independent of any other event in the system.

For recombination of multiple pairs of radicals, the probability of an event does depend on the history of the events on the chain. In a sense, the chain resembles a reactor containing many molecules of reactant A where a reaction of A + A takes place. Therefore, it seems that a reaction model assuming a second-order rate−concentration relationship shall be appropriate to describe the system. The latter approach has been used to describe the kinetic data in previous experimental works on intramolecular radical recombination. Please note that second-order kinetics is followed also by the intermolecular side reaction. We checked whether eq 3 (equivalent to eq 1 with second-order rate coefficient k) allows for a reasonably good description of radical recombination kinetics also in the present case. We made an attempt to fit both the simulation and experimental data for $N = 1068$ (see Figure 17) by applying eq 3. Results are shown in Figure 20.

This model can reproduce both the experimental and simulation data reasonably well, at least in the short and medium time range (the region of low Z, corresponding to long reaction times, is anyway hard to access experimentally).

Conclusions

Monte Carlo simulations of intramolecular recombination of polymer radicals provide information on the role of different parameters and phenomena in kinetics of nanogel formation.

- The average number of segments separating the radicals is the most important factor influencing the rate of recombination. Some influence on the total chain length is also observed, but it fades away for chains about twice as long as the interradical distance.
- In the case of single pair recombination, for fixed initial distances between radicals both along the chain and in space, the radical decay follows classical first-order kinetics. In the case of randomly generated radicals, the distribution of the interradical distances is the factor responsible for nonhomogeneous kinetics.

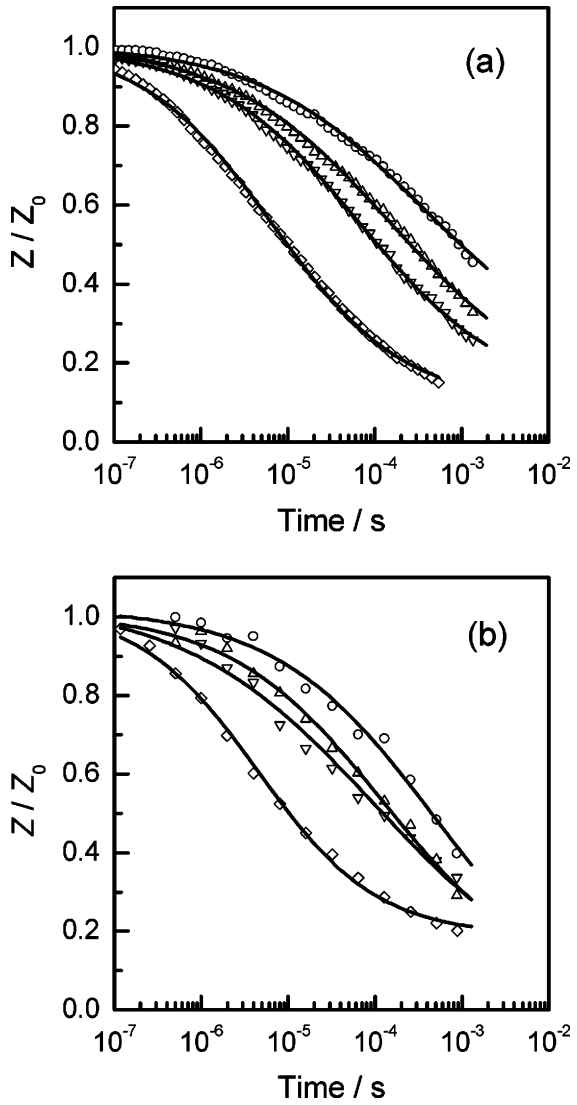

Figure 20. Fitting the data for $N = 1068$ (see Figure 17) with eq 3. Curves represent fits to (a) simulation data (symbols, Z_0: ◇, 20; ▽, 8; △, 6; ○, 4. α values: 0.57, 0.51, 0.46 and 0.45, respectively) and (b) experimental data for Z_0: ◇, 21.0; ▽, 7.2; △, 6.0; ○, 4.1 (α values: 0.63, 0.40, 0.49, and 0.46, respectively).

- Although the recombination kinetics is related to chain dynamics (which in turn depend on N_R and N), in almost all cases the radical decay half-time and time dependence are significantly different from those of end-to-end vector autocorrelation function of the radical−radical subchain.
- Single-pair recombination of randomly generated radicals may be approximated with the "stretched exponential" (KWW) function, where $\beta = 0.7-0.5$ depending on the chain length.
- If more than two radicals are generated on a chain, the recombination process becomes more complicated because a given radical can in principle recombine with any other. The simulation results show, however, that the recombination with the nearest neighbor is strongly favored, in agreement with the observation that decay half-times and thus probabilities of recombination strongly depend on the radical density on chain [$t_{1/2} \sim (N/Z_0)^x$, where $x = 1.8-2.3$]. This mechanism leads to a complicated time dependence which can be in the first approximation fitted by a sum of two stretched exponentials. The first one can be considered as representing the nearest-neighbor recombination and the second one as representing the successive recombinations of the remaining radicals. Recombination of many randomly generated radicals may also be reasonably well described with dispersive kinetics model of Plonka with a time-dependent second-order rate constant (eq 3).
- In contrast with a hypothesis formulated in some earlier experimental studies, simulation data indicate that formation of intramolecular covalent bonds during the recombination process (generation of loops) has no detectable influence on the radical decay kinetics when compared with cross-link-free disproportionation reaction, at least in the conditions tested in this work. This is caused by simultaneous occurrence of two opposite phenomena: loops cause a steric hindrance—slowing down recombination but formation of a loop decreases the distances between the radicals thus accelerating their recombination.
- Good agreement between of the results of pulse radiolysis experiments on PEO and MC simulations of the chain dynamics-controlled radical recombination indicate that the assumed simulation model can be used to gain insight into real systems. Considerable difference between the simulation and experiment is observed only for small number of radicals per chain, where side reactions (intermolecular recombination and radical transfer) modify the experimentally observed kinetics.

Recombination kinetics has also important implications for the structure of the final product (nanogel—internally cross-linked macromolecule) because formation of a bond with kinetically favored radical on a chain determines its topology. These issues will be dealt with in a separate paper.

Acknowledgment. The authors express their gratitude to the late professor Tadeusz Pakula (Max-Planck Institute for Polymer Research, Mainz, Germany) for making available the basic code of chain motion and valuable discussions as well as to the LINAC staff headed by Dr. Krzysztof Hodyr (TU Lodz) for their skilful technical assistance. This work has been supported in part by the Ministry of Science and Information Society Technologies, Poland (3 T08E 078 29), International Atomic Energy Agency (TCP POL/6/007), and NATO (PST.MEM.CLG 980622).

References and Notes

(1) Rosiak, J. M. In *Radiation Effects on Polymers*; Clough, R. C., Shalaby, S. W., Eds.; ACS Book Series; American Chemical Society: Washington, DC, 1991; Vol. 475, p 271.
(2) von Sonntag, C. *Radiat. Phys. Chem.* **2003**, *67*, 353−359.
(3) Ulanski, P.; Janik, I.; Rosiak, J. M. *Radiat. Phys. Chem.* **1998**, *52*, 289−294.
(4) Wang, B.; Mukataka, S.; Kodama, M.; Kokufuta, E. *Langmuir* **1997**, *13*, 6108−6114.
(5) Arndt, K.-F.; Schmidt, T.; Reichelt, R. *Polymer* **2001**, *42*, 6785−6791.
(6) Kadlubowski, S.; Grobelny, J.; Olejniczak, W.; Cichomski, M.; Ulanski, P. *Macromolecules* **2003**, *36*, 2484−2492.
(7) Funke, W.; Okay, O.; Joos-Müller, B. *Adv. Polym. Sci.* **1998**, *136*, 139−234.
(8) Langer, R. *Nature (London)* **1998**, *392 (Suppl.)*, 5−10.
(9) Saatweber, D.; Vogt-Birnbrich, B. *Prog. Org. Coat.* **1996**, *28*, 33−41.
(10) Pelton, R. *Adv. Colloid Interface Sci.* **2000**, *85*, 1−33.
(11) Ulanski, P.; Rosiak, J. M. In *Encyclopedia of Nanoscience and Nanotechnology*; Nalwa, H. S., Ed.; American Scientific Publishers: Stevenson Ranch, CA, 2004; Vol. VIII, p 845.
(12) Ulanski, P.; Zainuddin; Rosiak, J. M. *Radiat. Phys. Chem.* **1995**, *46*, 917−920.
(13) Sabharval, S.; Mohan, H.; Bhardwaj, Y. K.; Majali, A. B. *J. Chem. Soc., Faraday Trans.* **1996**, *92*, 4401−4406.
(14) Ulanski, P.; Rosiak, J. M. *Nucl. Instrum. Methods Phys. Res. B* **1999**, *151*, 356−360.
(15) Sabharval, S.; Mohan, H.; Bhardwaj, Y. K.; Majali, A. B. *Radiat. Phys. Chem.* **1999**, *54*, 643−653.
(16) Ulanski, P.; Kadlubowski, S.; Rosiak, J. M. *Radiat. Phys. Chem.* **2002**, *63*, 533−537.
(17) Alexander, P.; Charlesby, A. *J. Polym. Sci.* **1957**, *23*, 355−375.
(18) *Pulse Radiolysis*; Academic Press: London, 1965.

(19) Tabata, Y. *Pulse Radiolysis of Irradiated Systems*; CRC Press: Boca Raton, FL, 1991.
(20) von Sonntag, C.; Schuchmann, H.-P. *Methods Enzymol.* **1994**, *233*, 3−20.
(21) von Sonntag, C. *The Chemical Basis of Radiation Biology*; Taylor and Francis: London, 1987.
(22) Borgwardt, U.; Schnabel, W.; Henglein, A. *Makromol. Chem.* **1969**, *127*, 176−184.
(23) Schnabel, W. In *Proceedings of 10th Conference on Radioisotopes*, Japan Atomic Industral Forum: 1971; p 393.
(24) Plonka, A. *Prog. React. Kinet.* **1991**, *16*, 157−333.
(25) Plonka, A. *Dispersive Kinetics*; Kluwer Academic Publishers: Dordrecht, 2001.
(26) Ulanski, P.; Bothe, E.; Rosiak, J. M.; von Sonntag, C. *Makromol. Chem.* **1994**, *195*, 1443−1461.
(27) Ulanski, P.; Bothe, E.; Hildenbrand, K.; Rosiak, J. M.; von Sonntag, C. *J. Chem. Soc., Perkin Trans. 2* **1996**, 13−22.
(28) Janik, I.; Kujawa, P.; Ulanski, P.; Rosiak, J. M. *J. Chim. Phys.* **1997**, *94*, 244−250.
(29) Janik, I.; Ulanski, P.; Hildenbrand, K.; Rosiak, J. M.; von Sonntag, C. *J. Chem. Soc., Perkin Trans. 2* **2000**, 2041−2048.
(30) Rosiak, J.; Olejniczak, J.; Pekala, W. *Radiat. Phys. Chem.* **1990**, *36*, 747−755.
(31) Safrany, A.; Wojnarovits, L. *Radiat. Phys. Chem.* **2003**, *67*, 707−715.
(32) Safrany, A.; Wojnarovits, L. *Radiat. Phys. Chem.* **2004**, *69*, 289−293.
(33) Behar, D.; Rabani, J. *J. Phys. Chem.* **1988**, *92*, 5288−5292.
(34) Ulanski, P.; Bothe, E.; Hildenbrand, K.; von Sonntag, C. *Chem.−Eur. J.* **2000**, *6*, 3922−3934.
(35) Gauger, A.; Pakula, T. *Macromolecules* **1995**, *28*, 190−196.
(36) Pakula, T. *Macromolecules* **1987**, *20*, 679−682.
(37) Pakula, T.; Geyler, S. *Macromolecules* **1987**, *20*, 2909−2914.
(38) Pakula, T.; Jeszka, K. *Macromolecules* **1999**, *32*, 6821−6830.
(39) Pakula, T. *Rec. Res. Devel. Polym. Sci.* **1996**, *1*, 101.
(40) Pakula, T.; Geyler, S.; Edling, T.; Boese, D. *Rheol. Acta* **1996**, *35*, 631−644.
(41) Reiter, J. *J. Chem. Phys.* **1991**, *94*, 3222−3228.
(42) Geyler, S. Ph.D. Thesis, University of Mainz, 1990.
(43) Borodin, O.; Bedrov, D.; Smith, G. D. *Macromolecules* **2001**, *34*, 5687−5693.
(44) Heatley, F.; Walton, I. *Polymer* **1976**, *17*, 1019−1020.
(45) von Sonntag, C.; Bothe, E.; Ulanski, P.; Adhikary, A. *Radiat. Phys. Chem.* **1999**, *55*, 599−603.
(46) Buxton, G. V.; Greenstock, C. L.; Helman, W. P.; Ross, A. B. *J. Phys. Chem. Ref. Data* **1988**, *17*, 513−886.
(47) Teraoka, I. *Polymer Solutions. An Introduction to Physical Properties*; Wiley: New York, 2002.
(48) Kadlubowski, S. Ph.D. Thesis, Technical University of Lodz, 2004.
(49) Görlich, W.; Schnabel, W. *Makromol. Chem.* **1973**, *164*, 225−235.
(50) Ulanski, P.; Bothe, E.; Hildenbrand, K.; von Sonntag, C.; Rosiak, J. M. *Nukleonika* **1997**, *42*, 425−436.

MA0518757